

TURBULENT FLAME DYNAMICS OF HOMOGENEOUS SOLID PROPELLANT IN A ROCKET MOTOR

SOURABH APTE AND VIGOR YANG

*The Pennsylvania State University
University Park, PA 16802, USA*

A comprehensive numerical analysis has been conducted to study the combustion of a double-base homogeneous propellant in a rocket motor. Emphasis was placed on the motor internal flow development and its influence on propellant combustion. The formulation is based on the Favre-averaged, filtered equations for the conservation laws and takes into account finite-rate chemical kinetics and variable thermophysical properties. Turbulence closure is obtained using the large-eddy-simulation technique. The contribution of large energy-carrying structures to mass, momentum, and energy transfer is computed explicitly, and the effect of small scales of turbulence is modeled. The governing equations and associated boundary conditions are solved using a time-accurate, semi-implicit Runge-Kutta scheme coupled with a fourth-order central difference algorithm for spatial discretization. The motor internal flowfield is basically determined by the balance between the inertia force and the pressure gradient arising from the mass injection at the propellant surface. The temporal evolution of the vorticity field shows a laminar upstream region, a transition zone in the midsection of the chamber, and a fully developed turbulent regime further downstream. The turbulent mixing proceeds at a rate faster than chemical reactions, and the flame stretch is strong enough to regard propellant combustion as a well-stirred reactor. The combustion wave in the laminar region exhibits a two-stage structure consisting of a primary flame, a dark zone, and a secondary luminous flame. The enhanced energy and mass transport in the turbulent region partially merges the primary and secondary flames, thereby raising the temperatures in the dark zone. In the present study, the smoother axial velocity gradient and vertical flow convection prevent turbulence from deeply penetrating into the primary flame zone. The turbulence energy spectra indicate dominant harmonics in a frequency range capable of triggering combustion instabilities.

Introduction

Much of the research in the field of solid-propellant rocket propulsion is directed toward a clear understanding of the combustion instability phenomenon. The interactions among the mean, turbulent, and acoustic flowfields within the combustion chamber, and their effect on the physiochemical processes occurring in the thin flame region immediately above the burning propellant surface, can sustain high levels of pressure fluctuations leading to inefficient operation of the motor. Hence, a comprehensive study of the mutual coupling between the motor flow development and propellant combustion dynamics is essential. The present analysis deals with the homogeneous propellant combustion in a cylindrical chamber by means of a large-eddy-simulation (LES) technique. The large energy-carrying flow structures are resolved accurately, and the effect of small scales of turbulence is modeled. Emphasis is placed on the gas-phase flame dynamics in order to explore the effect of local flow motions on propellant burning.

Considerable progress was made by Tseng and Yang [1] in investigating the combustion of homogeneous propellants in realistic motor environments.

The issue of turbulence penetration into various flame zones and its ensuing influence on propellant burning behavior was carefully addressed. Roh et al. [2,3] conducted a comprehensive numerical study of the interactions between acoustic oscillations and transient propellant combustion in laminar flows, to identify the key mechanisms responsible for driving instabilities. The model also featured a finite-rate chemical kinetic mechanism involving five rate-limiting reactions in the gas phase and two reactions in the condensed phase to resolve the detailed combustion wave structure. The instantaneous burning rate was treated as part of the solution. The same analysis was later extended to incorporate the effect of turbulence [4,5]. Results indicate that the oscillatory flow characteristics were significantly altered due to the turbulence-enhanced mass and energy transport in the gas phase. As a consequence, the energy released in the flame zone and the propellant combustion response were modified, leading to a qualitative change in the motor stability behavior.

All the previous studies in the fields of solid propellant combustion and rocket motor internal flows employed conventional Reynolds-averaging techniques for turbulence closure. Although these closure schemes provide good insight into propellant

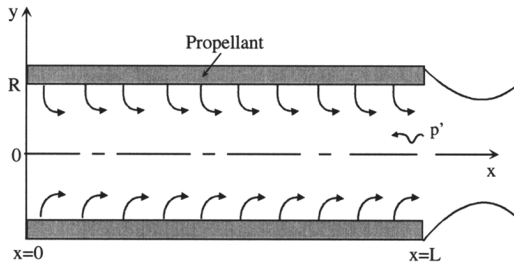


FIG. 1. Schematic diagram of a solid rocket motor.

flame dynamics, they are based on semi-empirical data and lack generality. The schemes provide little information about the wide range of turbulent energy and dissipation spectra and are insufficient to explore the intricate interactions among the acoustic, vortical, and entropy waves produced in a rocket chamber. The present work is the first attempt to apply higher-order closure schemes based on LES techniques to study these processes in depth, and it lays the foundation to further advance the knowledge base. This analysis has been previously applied to study of the non-reacting flowfield in simulated nozzleless rocket motors [6] and was carefully validated against the experimental data [7]. The work was further advanced to simulate traveling acoustic oscillations in a chamber with mass injection [8]. The energy transfer mechanisms among the mean, turbulent, and acoustic flows were investigated in depth, instigating its application to the present study with propellant combustion.

Theoretical Formulation

Figure 1 shows the physical model of concern, an axisymmetric combustion chamber loaded with a double-base propellant grain and connected downstream to a choked exhaust nozzle. The propellant undergoes degradation in a thin superficial layer underneath the burning surface. The gaseous pyrolysis products are injected into the combustion chamber along the azimuth, and then react to form the primary and secondary flames in the gas phase. Because of the intricacy of the problem, which involves a wide range of length and time scales, and the limitation of computational resources, the analysis deals only with the conservation laws in axisymmetric coordinates. This treatment lacks the vortex-stretching phenomenon commonly observed in turbulent flows and may underpredict the turbulence production and dissipation rates. The model, nonetheless, allows for a systematic investigation into the interactions between propellant combustion and motor flow development. Much useful information can be obtained about the effect of turbulence on flame dynamics, especially in the near-surface region. A

recent study of rocket motor internal flow based on a comprehensive three-dimensional, LES technique [9] indicated that the two-dimensional simulation can indeed capture the salient features of turbulent flows and leads to good agreement with experimental data in terms of mean flow properties and acoustic-wave-induced flow oscillations.

The governing equations in axisymmetric coordinates can be written conveniently in the following vector form:

$$\frac{\partial \mathbf{Q}}{\partial t} + \frac{\partial}{\partial x} (\mathbf{E} - \mathbf{E}_v) + \frac{\partial}{\partial y} (\mathbf{F} - \mathbf{F}_v) = \mathbf{H} \quad (1)$$

where x and y represent the axial and radial coordinates, respectively. The inviscid flux vectors, \mathbf{E} and \mathbf{F} , and the viscous flux vectors, \mathbf{E}_v and \mathbf{F}_v , follow the definitions given in Ref. [5]. The vector of conserved variables \mathbf{Q} is defined as

$$\mathbf{Q} = y[\rho, \rho u, \rho v, \rho e, \rho Y_i]^T \quad (2)$$

The source term \mathbf{H} includes contributions from chemical reactions and the axisymmetric treatment of flow properties. A reduced chemical kinetics mechanism comprising two global reactions in the condensed phase and five reactions in the gas phase is employed to describe the combustion-wave structure [2].

Turbulence Modeling

Turbulence closure is obtained based on the LES technique in which large, energy-carrying structures are computed explicitly and the effect of small-scale motions on large scales is modeled. A spatial filter G is employed to decompose the flow variables into a large (resolved) and a subgrid (unresolved) scale,

$$\begin{aligned} \mathcal{F}(\mathbf{x}, t) &= \mathcal{F}^r(\mathbf{x}, t) + \mathcal{F}^s(\mathbf{x}, t) \text{ with} \\ \mathcal{F}^r(\mathbf{x}, t) &= \int_D G(\mathbf{x} - \mathbf{x}', \Delta) \mathcal{F}(\mathbf{x}', t) d^3x' \end{aligned} \quad (3)$$

where D is the entire domain, Δ is the computational mesh size which determines the size and structure of the unresolved scales, and \mathcal{F} is any flow property ρ , u , v , T , or Y_i . The superscripts r and s represent the resolved and unresolved scales of flow properties, respectively. Favre averaging is further used to simplify the governing equations for a compressible turbulent-flow simulation [10]. This density-weighted averaging eliminates complex triple correlations between density and velocity fluctuations in the governing equations and is given as

$$\tilde{\mathcal{F}}^r = \frac{\langle \rho \mathcal{F}^r \rangle}{\rho^r} \quad (4)$$

The filtered forms of the governing equations for axisymmetric configurations are obtained to compute the large-scale motions explicitly. The effect of

unresolved scales is modeled to provide adequate dissipation by means of the Smagorinsky model [11]. A comprehensive description of formulation is given in Ref. [12].

Turbulence/Chemistry Interaction

The reaction rates $\dot{\omega}_i$ in the species-concentration equations need to be modeled in order to capture the effect of subgrid scales on the chemistry. Peters [13] examined the problem of turbulence/chemistry interactions for premixed flames in terms of three non-dimensional parameters: turbulent Reynolds number, Re_t , turbulent Damkohler number, Da , and turbulent Karlovitz number, Ka , as defined in Ref. [1]. If chemical reactions proceed at rates lower than those of turbulent mixing (i.e., $Da < 1$), and the flame stretch is strong enough to cause penetration of small eddies into the flame zone (i.e., $Ka > 1$), then the flame structure can be locally modeled as a well-stirred reactor. Under this situation, turbulence rapidly penetrates into the flame zone through enhanced mass transfer, leaving chemical reactions as the rate-controlling processes. No direct interactions between turbulence and combustion occur in this regime. The present analysis indicates that, for the combustion of homogeneous double-base propellant, the condition of $Ka > 1$ and $Da < 1$ is always satisfied in the flame zone, a situation first observed by Tseng and Yang [1]. Accordingly, the closure for reaction rates follows the usual approximation of resolved reaction rates [11]:

$$\begin{aligned}\dot{\omega}_i^r &= \dot{\omega}_i^r(\rho, T, Y_1, Y_2, \dots, Y_N) \\ &= \dot{\omega}_i(\rho^r, \tilde{T}^r, \tilde{Y}_1^r, \tilde{Y}_2^r, \dots, \tilde{Y}_N^r)\end{aligned}\quad (5)$$

The above model allows for fluctuations in the production rates as functions of instantaneous flow properties and thus is less stringent compared to that used in second-order turbulence-closure schemes [1].

Boundary Conditions

The present work focuses on the gas-phase flame dynamics, with the propellant surface conditions specified based on their values at the chamber head end [2]. Accordingly, the burning rate, surface temperature, and species concentrations remain fixed throughout the entire motor. This assumption of uniform distribution is in part justified by the experimental observations [14,15] that in many cases, the erosive burning effect occurring in a strong turbulent environment offsets the decrease in burning rate due to reduced pressure in the downstream region and as a result no discernible variation of propellant burning rate is obtained. The issue of propellant combustion response to local flow variation is currently being addressed in a companion study.

According to the method of characteristics, the exit plane requires no physical boundary condition, since the flow is supersonic downstream of the nozzle throat. At the upstream boundary, the axial velocity and pressure gradient, as well as the radial velocity gradient, are set to zero along the solid wall. The last condition is required to prevent the occurrence of a numerically produced recirculating flow at the head end. The mass burning rate, total temperature, and species mass fluxes are fixed at the propellant burning surface. Normal injection of the pyrolysis products is enforced by employing the no-slip condition. Finally, flow symmetry is assumed at the centerline.

Numerical Method

One characteristic trait of solid-propellant rocket motor internal flowfields is that the Mach number varies from zero at the head end to unity in the nozzle throat section as the flow accelerates rapidly in the downstream region. In the low Mach-number region, the inviscid compressible form of the conservation equations is poorly coupled and stiff [1]. The associated disparity among the eigenvalues results in significant slowdown of the numerical convergence rate. Chemical reactions exhibit another category of numerical difficulties because of the wide range of time and length scales involved in their computations. In regions where reaction rates are high, the species concentrations may vary rapidly over a short period of time, and the chemical source terms must be treated implicitly to avoid numerical instabilities. To circumvent the above difficulties, a preconditioning technique along with a dual-time stepping integration procedure described in Ref. [16] is first used until the initial transients in the flowfield diminish and a stable flame is established. However, the preconditioning method is computationally expensive and difficult to parallelize because of its implicit form. A time-accurate semi-implicit Runge-Kutta scheme with fourth-order central differencing for spatial discretization is then employed for unsteady flow computations. The scheme is further equipped with the properties of matrix dissipation and total-variation-diminishing (TVD) switches to accurately capture steep temperature and density gradients in the flame region [17,18]. The computational domain is decomposed into small cylindrical blocks to facilitate parallel processing and message passing. The simulation was performed on a single-instruction-multiple-data (SIMD) cluster of 30 Pentium II nodes and required 7200 CPU-processor hours to obtain statistically meaningful data over a time period of 6 ms.

Results and Discussion

The gas-phase combustion dynamics of homogeneous propellant in an axisymmetric motor has been

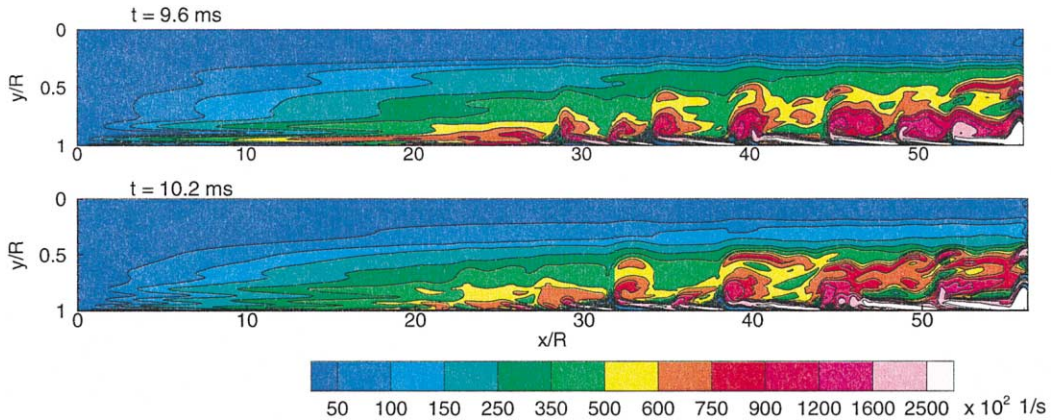


FIG. 2. Time evolution of vorticity field.

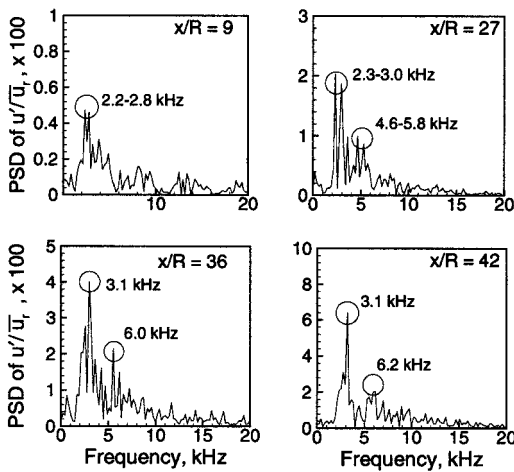


FIG. 3. Power spectral density of axial velocity fluctuation at various axial locations, $y/R = 0.98$.

investigated using the analysis described earlier. The major ingredients of the propellant are 52% nitrocellulose, 43% nitroglycerine, and 5% additives, simulating one of the propellants (code number EC-1) studied by Kubota et al. [19]. The chamber measures 2 cm in diameter and 55 cm in length and is connected to a choked nozzle at the exit, as shown in Fig. 1. The nozzle throat area is set based on the contraction ratio of 1.25. The low contraction ratio gives rise to higher Mach numbers in the downstream region of the chamber, such that the effect of high-speed cross flow on flame dynamics can be studied. The chamber pressure is 25 atm and the flame thickness is 5 mm at the head end. The mass flux at the propellant surface is $8.1 \text{ kg/m}^2\text{s}$, with the injection Reynolds and Mach numbers around 10^4 and 1.85×10^{-3} , respectively. The surface temperature is fixed at 640 K. The computational grid

consists of 500 and 130 points in the axial and radial directions, respectively. The grid is highly stretched toward the propellant burning surface to accurately resolve the flame structure and steep temperature gradients near the surface. The smallest grid spacing normal to the surface is about $10 \mu\text{m}$.

Vorticity Dynamics

Figure 2 shows the temporal evolution of the vorticity field. Only the lower half of the cylindrical chamber is presented to facilitate discussion, where $y/R = 1$ corresponds to the burning surface. Vorticity is produced at the propellant surface because the no-slip condition renders the flow to enter the chamber radially and then turn to align smoothly with the axial axis [20]. Near the head end, the turbulent fluctuations appear to be small, and the flow is mostly laminar. Transition to turbulence occurs around $x/R = 25$, and the flow becomes highly turbulent further downstream. In an axisymmetric flow without heat release or viscous effects, the vorticity of a given fluid particle is conserved. However, the conservation property of vorticity is no longer valid due to viscous dissipation, volume dilatation, and baroclinicity resulting from the misalignment between the density and pressure gradients. In the flame zone, density varies dramatically so that volume dilatation and baroclinicity become predominant and viscous dissipation gives negligible contribution to the vorticity evolution. The present axisymmetric computation lacks the vortex-stretching phenomenon responsible for transfer of energy from the large to the small scales through the energy cascade mechanism, and leads to lower dissipation and production rates. Nevertheless, it provides much useful insight into the flow development and its interactions with the propellant flame dynamics, which was not previously available using second-order turbulence closure schemes.

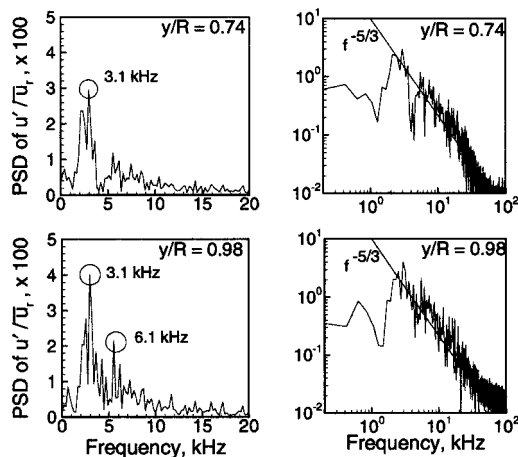


FIG. 4. Power spectral density of axial velocity fluctuation at various radial locations, $x/R = 40$.

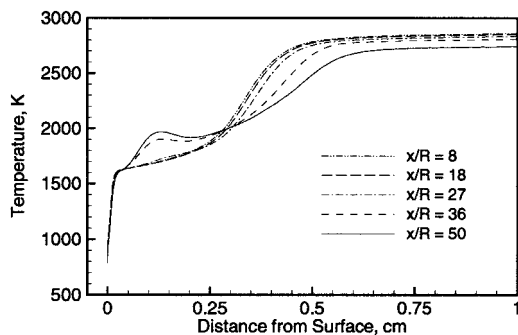


FIG. 5. Radial distributions of temperature at various axial locations.

Figure 3 shows the power spectral density of axial velocity fluctuations (u') at various axial locations, normalized with the reference velocity (\bar{u}_r) corresponding to the mean centerline velocity at Mach number 0.6. Here, the fluctuating variable is obtained by subtracting the time-mean value from its instantaneous quantity. The peak magnitude of u' increases as the flow accelerates in the axial direction. The range of dominant harmonics containing most of the turbulence intensity varies according to the local Reynolds number. The vortex-shedding frequencies (i.e., 3.1 and 6.1 kHz) correspond to the natural hydrodynamic instability modes. Turbulence induces low-frequency fluctuations in pressure (not shown) in the downstream region with frequencies of the order of the first and second longitudinal acoustic modes of the motor (i.e., 850 and 1900 Hz). This suggests a mechanism for strong coupling between the acoustic motions and turbulence. A comprehensive analysis of the interactions among the acoustic, vortical, and entropy waves produced

within the combustion chamber is currently being performed and will be presented in subsequent publications. Following the data analysis procedure established in Ref. [8], the present work could be used effectively to identify various motor instability phenomena.

Figure 4 shows the energy spectra of u' at two radial locations in the fully turbulent regime, $x/R = 40$. The decrease in the dominant frequency away from the surface is indicative of the vortex-pairing phenomenon commonly observed in turbulent shear flows. An upstream vortical disturbance originating close to the wall overtakes a neighboring downstream disturbance since it is convected at a higher speed. As these vortical structures travel away from the wall, their size doubles, and therefore the frequency is halved [21]. The energy spectra are also shown on a log-log scale and compared with the Kolmogorov-Obukhov spectrum ($-5/3$ law) obtained for homogeneous turbulence at large Reynolds numbers. The cut-off frequency of the present calculation lies in the inertial subrange, ensuring that the large-scale motions are correctly resolved.

Mean Flowfield

The mean flowfield is obtained by taking the time average of the instantaneous quantities over 6 ms in order to obtain statistically meaningful data. The mean Mach number increases along the centerline almost linearly from zero at the head end to 0.6 at the nozzle entrance, and the flow becomes supersonic in the divergent section of the nozzle [12,22]. The flowfield clearly exhibits a multidimensional structure with the Mach number near the surface having a much smaller value. The situation with pressure, however, is substantially different. The pressure decreases from the head end to the nozzle exit as the flow accelerates due to the propellant burning. The flowfield is dominated by the axial strain rates, and variations in the radial velocity are so small that an almost uniform distribution of the chamber pressure in the radial direction is obtained [1–5,8]. A comprehensive description of the mean flowfield can be obtained from Refs. [12,22].

Turbulence and Flame Dynamics

The radial distributions of the mean temperature at various axial locations is shown in Fig. 5. A two-stage flame structure consisting of the primary flame, the dark zone, and the secondary-flame zone is clearly observed in the upstream laminar region [2]. The temperature increases rapidly from 640 K at the surface to around 1600 K in the dark zone, and reaches the final flame temperature of 2850 K. The overall reaction mechanism for the propellant burning can be globally grouped into the following steps: (1) molecular degradation and ensuing exothermic

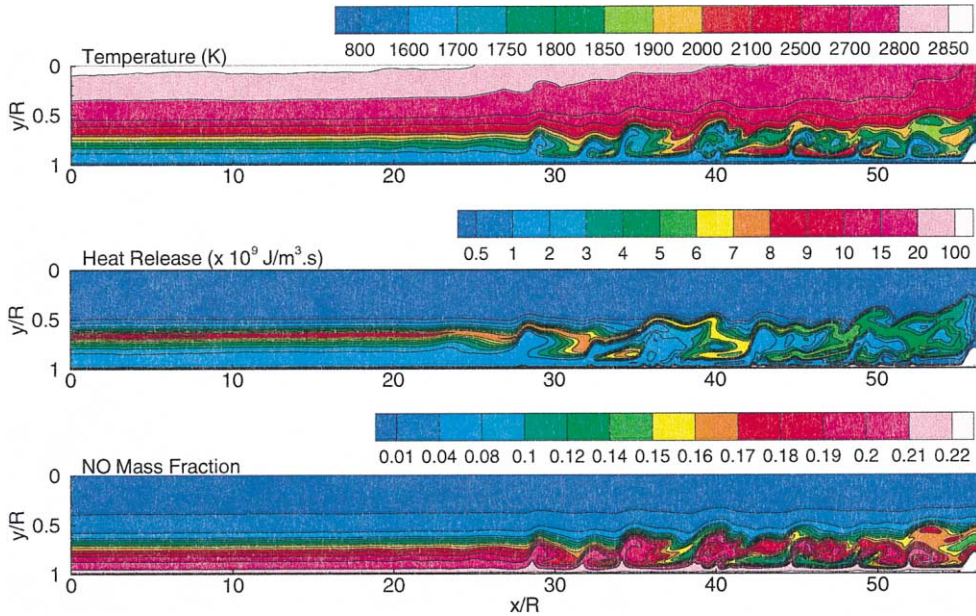


FIG. 6. Snapshots of temperature, heat release, and NO mass fraction fields, $t = 9.6$ ms.

reactions of NO_2 and aldehydes in the subsurface layer; (2) generation of NO , CO , CO_2 , and H_2O , as well as removal of NO_2 and aldehydes, in the primary flame; and (3) reduction of NO to form the final products such as N_2 , CO_2 , H_2 , and so forth in the secondary flame [2]. The thickness of the dark zone depends on the chemical reaction time and the flow convection time determined by the radial velocity distribution. In the turbulent region, the enhanced thermal diffusion facilitates the NO reduction, which normally occurs at elevated temperatures due to its large activation energy. This process leads to a rapid temperature rise at the end of the primary flame and, consequently, a thinner dark zone. The temperature plateau around 2000 K may result from the increased radial velocity, which essentially reduces the local flow-residence time required for completing chemical reactions.

The radial variations of the turbulence intensity (not shown) at various axial locations were computed from the collected data [12,22]. Several points should be noted here. First, the onset of turbulence occurs in regions away from the propellant surface due to the stronger local hydrodynamic instability. The peak of turbulence intensity tends to move away from the primary flame zone along the chamber. One factor contributing to this phenomenon is the intricate coupling among the flow convection, chemical reaction, and turbulent mixing in the downstream flame zone. Second, since the flow is dominated by strain rates in the axial direction, the axial turbulence intensity appears to be much greater

than its radial counterpart. Third, in the present study, the chamber pressure is 25 atm at the head end, which is much lower than the pressure of 65 atm studied in Ref. [1]. The resultant mass burning rate and injection Reynolds number are so small that the turbulence intensity near the surface is too weak to exercise any influence on the flame structure. Hence, the mean temperature profile in the primary flame zone remains unchanged even in the turbulent regime.

Evolution of Temperature, Heat Release, and Species Mass Fraction

The temporal evolution of the temperature field and its associated heat-release distribution was obtained to provide direct insight into the turbulent combustion mechanism. Fig. 6 shows the snapshots of the temperature, total heat-release, and NO mass-fraction fields. For the present configuration, the Karlovitz number, Ka , characterizing the turbulent flame stretch as the ratio of the chemical time scale to the Kolmogorov time scale is larger than unity throughout the entire flame zone. This leads to a highly stretched and thickened flame. Small turbulent eddies can penetrate into the secondary flame zone and cause large temperature oscillations in the turbulent regime. The heat-release fluctuation basically follows the spatial gradient of the temperature fluctuation and can be easily determined by the energy balance over a control volume [2]. A large

amount of heat is released in the primary and secondary flame zones. The rapid fluctuations of temperature and heat release suggest strong interactions between the flame dynamics and flow evolution. The consumption of NO in the secondary flame zone is a rate-limiting reaction for homogeneous propellant combustion. The turbulence-enhanced heat and mass transport results in rapid reduction of NO in the dark zone, thereby releasing a large amount of energy and increasing local flame temperature. Small fluctuations in temperature, heat release, and species concentrations are also observed in the primary flame zone very close to the burning surface. This elucidates the potential of the present work in analyzing the intricate physiochemical processes occurring in the near-surface flame zone and their effect on transient propellant combustion responses in realistic motor environments.

Conclusion

The gas-phase flame dynamics of a double-base homogeneous solid propellant in an axisymmetric rocket motor has been investigated in depth. Turbulence closure was obtained by means of a LES technique for the first time to allow for a comprehensive analysis of the interactions between propellant combustion and motor flow development. Results indicate that the temperature distribution in the flame zone exerts a significant influence on the flow evolution. The effect of turbulence appears mainly in determining eddy diffusivity and conductivity, and propellant combustion can be treated as a well-stirred reactor. The propellant combustion in the upstream laminar region exhibits a two-stage flame structure similar to that observed in a stationary environment. The enhanced heat and mass transfer in the downstream turbulent region elevates the temperatures in the dark zone and consequently decreases the dark zone thickness. The primary flame structure is little affected in the present study because the smoother axial velocity gradient and vertical flow convection prevent turbulence from deeply penetrating into the primary flame. Spectral analysis of the turbulence properties indicates potential mechanisms for driving combustion instabilities.

Nomenclature

\mathbf{E}, \mathbf{F}	convective flux vectors
$\mathbf{E}_v, \mathbf{F}_v$	diffusive flux vectors
e	specific total energy
G	spatial filter
\mathbf{H}	source vector
N	number of species in gas-phase reactions
\mathbf{Q}	dependent variable vector
R	chamber radius

T	temperature
t	time
u, v	bulk velocities in axial and radial directions, respectively
x, y	axial and radial coordinates
Y_i	mass fraction of species i
Δ	filter width
ρ	density
$\dot{\omega}_i$	rate of production of species i
<i>Superscripts</i>	
'	fluctuating quantity
r	resolved scale
s	subgrid scale
\sim	density-weighted quantity

Acknowledgments

This work was sponsored partly by The Pennsylvania State University and partly by the California Institute of Technology Multidisciplinary University Research Initiative under ONR grant no. N00014-95-1-1338.

REFERENCES

1. Tseng, I. S., and Yang, V., *Combust. Flame* 96:325–342 (1994).
2. Roh, T.-S., Tseng, I. S., and Yang, V., *J. Propul. Power* 11:640–665 (1995).
3. Roh, T.-S., Apte, S. V., and Yang, V., *Proc. Combust. Inst.* 27:2335–2341 (1998).
4. Roh, T.-S., and Yang, V., AIAA paper 96-2623.
5. Roh, T.-S., Apte, S. V., and Yang, V., *Prog. Astronaut. Aeronaut.* 185:837–857 (2000).
6. Liou, T. M., and Lien, T. H., *J. Propul. Power* 14:282–289 (1998).
7. Traineau, J. C., Hervat, P., and Kuentzmann, P., AIAA paper 86-1447.
8. Apte, S. V., and Yang, V., *Prog. Astronaut. Aeronaut.* 185:791–819 (2000).
9. Apte, S. V., and Yang, V., AIAA paper 2000-0709.
10. Erlebacher, G., Hussaini, M. Y., Speziale, C. G., and Zang, T. A., ICASE technical report, paper 87-20, 1990.
11. DesJardin, P. E., and Frankel, S. H., *Phys. Fluids* 10:2298–2314 (1998).
12. Apte, S. V., "Unsteady Flow Evolution and Combustion Dynamics of Homogeneous Solid Propellant in a Rocket Motor," Ph.D. thesis, Department of Mechanical Engineering, The Pennsylvania State University, University Park, PA, December 2000.
13. Peters, N., in *Numerical Approaches to Combustion Modeling* (E. S. Oran and J. P. Boris, eds.), AIAA, Washington, D.C., 1991, pp. 155–182.
14. Nahon, S., AIAA paper 84-1312.
15. Traineau, J. C., and Kuentzmann, P., AIAA paper 84-1469.
16. Hsieh, S. Y., and Yang, V., *Int. J. Comp. Fluid Dynam.* 8:31–49 (1997).

17. Swanson, R. C., and Turkel, E., *J. Comp. Phys.* 101:292–306 (1992).
18. Jorgenson, P., and Turkel, E., *J. Comp. Phys.* 107:297–308 (1993).
19. Kubota, N., *Proc. Combust. Inst.* 17:1435–1441 (1979).
20. Flandro, G. A., *J. Propul. Power* 11:607–625 (1995).
21. Dunlap, R., Blackner, A. M., Waugh, R. C., Brown, R. S., and Willoughby, P. G., *J. Propul. Power* 6:690–704 (1990).
22. Apte, S. V., and Yang, V. “Coupling between Unsteady Flow Evolution and Transient Combustion of Homogeneous Propellant in a Rocket Motor,” in *Proceedings of Thirty-Seventh JANNAF Combustion Meeting*, 2000.

COMMENTS

Sebastien Candel, Ecole Centrale Paris, France. It was indicated in the presentation that the Damköhler number was less than unity. However, this number will change from section to section because the flow velocity changes from nearly zero to a high value. I was wondering how this number was established. I also noticed that the heat release was quite localized indicating that the flame was quite identifiable, apparently indicating that the regime at combustion may not be of the distributed reaction type.

Author's Reply. The Damköhler and Karlovitz numbers are computed as follows:

$$Da = \frac{k/\varepsilon}{\dot{\omega}_i/\rho}, \quad Ka = \frac{\dot{\omega}_i}{\rho} \sqrt{\frac{\varepsilon}{\nu}}$$

where k is the turbulent kinetic energy, ε the turbulent dissipation rate, ρ is the density, ν is the kinematic viscosity and $\dot{\omega}_i$ is the species mass production rate. These numbers vary in the axial direction, however, their radical distributions in the turbulent flame region always fall in the regime of $Da < 1$ and $Ka > 1$. The turbulent combustion may be locally treated as a well-stirred reactor. An in-depth analysis can be found in Refs. [12,22] in paper.

The thickness of the two-stage flame structure is large (0.3–0.4 cm) compared with the chamber radius ($R = 1$ cm), and thus the flame may not be considered as a flame sheet. The heat-release contours indicate an identifiable flame corresponding to the secondary flame zone. The propellant combustion response, however, is determined by the primary flame, which remains unaffected even in the turbulent regime for the present configuration.

Allen Kuhl, Lawrence Livermore National Laboratory, USA. Your numerical simulations are two-dimensional axisymmetric, but the vorticity distribution will be three-dimensional. In particular, the vorticity will evolve into streamwise filaments that generate mixing that is fundamentally different from your two-dimensional simulations. Therefore, care is suggested in interpreting your results quantitatively.

Author's Reply. The authors appreciate the suggestion. The present work represents the first attempt to incorporate finite-rate chemical kinetics to model the two-stage

flame structure of homogeneous solid-propellant combustion in rocket motors. As pointed out in the paper, the axisymmetric simulation lacks the vortex-stretching phenomenon commonly observed in turbulent flows and may underpredict turbulence production and dissipation rates [1]. A two-dimensional time-resolved simulation of non-reacting flows in a simulated nozzleless rocket motor, however, has been shown to capture the salient features of turbulent flows and led to good agreement with experimental data in terms of mean flow properties and acoustic-wave-induced flow oscillations (Refs. [9,12] in paper). The present work establishes a numerical/theoretical framework that can be easily extended to three-dimensional simulations.

REFERENCE

1. Apte, S. V., and Yang, V., *J. Fluid Mech.*, in press (2000).

Xu Zhou, Queen Mary and Westfield College, UK. You obtained a dominant frequency. Do you observe the Strouhal number $St = fD/U_0$ within any range? For example, for a jet flow, the jet-preferred mode of instability in terms of Strouhal number is $\sim 0.3\text{--}0.7$.

Author's Reply. Previous work on the flow evolution in simulated rocket motors under non-reacting conditions [1,2] indicated that the Strouhal number based on the injection velocity, chamber half-height, and dominant vortex-shedding frequency, $St = fh/v_w$, has a value around 6, corresponding to the pure hydrodynamic instability. For the present reaction-flow simulations, however, the presence of a distributed reaction zone significantly modifies the vorticity dynamics. The vortex-flame interactions become so important that the Strouhal number based on the above definition may not characterize the dominant frequencies observed in the fluctuation-velocity spectra.

REFERENCES

1. Apte, S. V., and Yang, V., *AIAA J.*, in press (2000).
2. Abalone, G., Ugurtas, B., Grith, F., and Bretton, A., *AIAA paper 2000-3387*, 2000.